

Pulmonary Vessel Segmentation using Vessel Enhancement Filters

Marius Staring^{1*}, Changyan Xiao², Denis P. Shamonin¹, and Berend C. Stoel¹

¹ Division of Image Processing (LKEB), Department of Radiology, Leiden University Medical Center, Leiden, The Netherlands

² College of Electrical and Information Engineering, Hunan University, Hunan, P.R. China

Abstract. The goal of the VESSEL12 challenge is to compare methods for automatic (and semi-automatic) segmentation of the vessels in the lungs from chest computed tomography scans taken from both healthy and diseased populations. The challenge has a workshop in conjunction with the ISBI 2012 conference.

We registered to the challenge with team LKEBChina. The goal of our submission is to determine what advanced and fully automatic vessel enhancement filters can achieve compared to the competition. We applied four different filters to the problem. All of them derive a vesselness function from the Hessian eigenvalues, and sometimes in addition the gradient magnitude. The first is the well known Frangi vesselness filter (V^{Frangi} , [1]), the second a medialness Hessian-based vesselness filter derived from work of Krissian and using a Gaussian kernel (V^{med} , [2]), the third a variation of the second using a bi-Gaussian kernel ($V_{\text{BG}}^{\text{med}}$, Xiao *et al.* [3]), and the fourth a filter based on stress-strain principles in mechanics (V^{SE} , Xiao *et al.* [4]). All filters are embedded in a multi-scale scheme. After the vesselness computation the response was converted to the range 0 - 255, as required by the organizers.

The algorithms were applied to 20 data sets provided by the organizers. Overall optimal specificity and sensitivity as reported by the organizers were (0.914, 0.960), (0.956, 0.953), (0.948, 0.953) and (0.941, 0.921), for V^{Frangi} , V^{med} , $V_{\text{BG}}^{\text{med}}$ and V^{SE} , respectively. The methods differed in their responses to sub-categories: V^{Frangi} was substantially underperforming on airways; $V_{\text{BG}}^{\text{med}}$ and V^{SE} performed best on dense abnormalities and bronchi; V^{SE} was less sensitive on vessels within dense abnormalities. Quite high scores were obtained for all filters.

Key words: pulmonary vessel segmentation, evaluation, strain energy density, shape discrimination

1 Introduction

The goal of our contribution is to determine what advanced, general purpose, and fully automatic vessel enhancement filters can achieve compared to the com-

* Corresponding author: m.staring@lumc.nl

petition. To this end we selected some existing vessel enhancement filters, our prior work, and added new ones.

2 Methods

All vessel enhancement filters below derive structural information from the Hessian eigenvalues $|\lambda_1| \leq |\lambda_2| \leq |\lambda_3|$. The Hessian \mathcal{H} is computed using Gaussian derivatives at a scale σ , except for the filter described in Section 2.3, where a new bi-Gaussian kernel is used. The Gaussian second order derivative of image I at scale σ and point x is given by

$$\frac{\partial^2 I_\sigma}{\partial x^2} = I(x) * \frac{\partial^2 G(\sigma, x)}{\partial x^2}. \quad (1)$$

All filters define a vesselness function $V(\sigma, x)$ and can be embedded in a multi-scale framework using

$$V(x) = \max_{\sigma} V(\sigma, x), \quad \sigma_{\min} < \sigma < \sigma_{\max} \quad (2)$$

All filters used in this paper are fully automatic, are applicable to any kind of vasculature data (not restricted to pulmonary vasculature), and do not require training. Most filters do have parameters, which were tuned by visual inspection.

2.1 Frangi vesselness

In his seminal 1998 paper [1] Frangi introduced three measures to describe structure in images: $R_B = |\lambda_1|/\sqrt{|\lambda_2\lambda_3|}$, $R_A = |\lambda_2|/|\lambda_3|$, and $\mathcal{S} = \|\mathcal{H}\|_F = \sqrt{\sum_i \lambda_i^2}$, which quantify deviation from a blob-like structure, the difference between plate-like and line-like structures, and background noise, respectively. These measures were combined in a vesselness function as:

$$V^{\text{Frangi}}(\sigma, x) = \begin{cases} 0 & \lambda_2, \lambda_3 > 0 \\ \left(1 - \exp\left(-\frac{R_A^2}{2\alpha^2}\right)\right) \cdot \exp\left(-\frac{R_B^2}{2\beta^2}\right) \cdot \left(1 - \exp\left(-\frac{\mathcal{S}^2}{2c^2}\right)\right) & \text{otherwise} \end{cases} \quad (3)$$

with α, β and c real-valued positive user-defined parameters.

2.2 Krissian-inspired vesselness

A second vesselness measure is inspired by the work of Krissian *et al.* [2]. They defined a central adaptive medialness for the detection of tubular structures, which we approximate by the sum of the two largest eigenvalues $\lambda_2 + \lambda_3$. They also showed that the ratio λ_2/λ_3 decreases from the center of a vessel. We combine this information in a new vesselness measure as follows:

$$V^{\text{med}}(\sigma, x) = \begin{cases} 0 & \lambda_1 + \lambda_2 + \lambda_3 \geq 0 \\ -\frac{\lambda_2}{\lambda_3} \cdot (\lambda_2 + \lambda_3) & \text{otherwise} \end{cases} \quad (4)$$

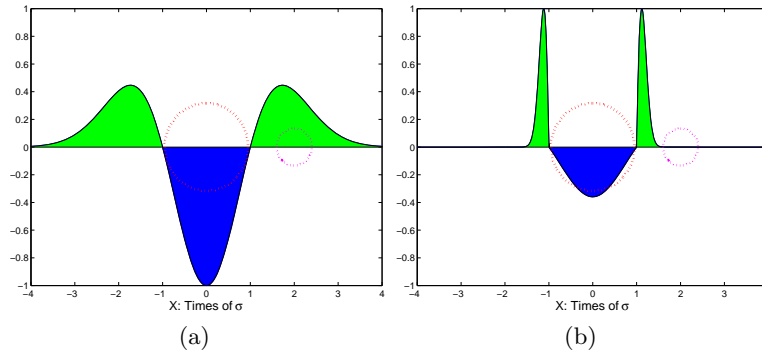


Fig. 1. Second order derivative of the Gaussian and the bi-Gaussian kernel. Here, the magnitudes of all the kernels are normalized to 1 for comparison, and the x coordinates are represented in multiples of scale σ . The big circles indicate the cross-sections of desired tubular objects, and the smaller circles denote adjacent disturbances.

Here, the sum of eigenvalues is used to define the contrast, which has a negative response to bright objects according to our previous work [4]. The two largest eigenvalues are used to measure the structure strength, and their ratio is multiplied to punish deviation from the tubular center. By omitting λ_1 , the filter tends to preserve axial continuity, since the intensity change in this direction is neglected.

2.3 Krissian-inspired vesselness using a bi-Gaussian kernel

The traditional Gaussian operator has infinite support and its response is therefore influenced by structures adjacent to a vessel. To avoid the problem, we propose [3] to replace the low-level Gaussian kernel with a bi-Gaussian function, which allows independent selection of foreground and background scales. By taking a narrower local neighborhood for contrast computation, the proposed method will obtain a good property in separating closely located adjacent structures, while keeping the intra-vessel region noise suppressing and size adapting ability of conventional Gaussian scale space.

The bi-Gaussian kernel takes the form

$$BG(\sigma, \sigma_b, x) = \begin{cases} k \cdot G(\sigma_b, x - \sigma_b + \sigma) & x \leq -\sigma \\ G(\sigma, x) + c & |x| < \sigma \\ k \cdot G(\sigma_b, x + \sigma_b - \sigma) & x \geq \sigma \end{cases} \quad (5)$$

where σ is the original scale used within the structure, and σ_b the background scale. The constants k and c are deduced to be $k = \sigma_b^2/\sigma^2$ and $c = \frac{e^{-1/2}}{\sqrt{2\pi}}(\sigma_b/\sigma - 1)/\sigma$, in order to fulfill some scale-space conditions. Additionally, we take a fixed ratio $\rho = \sigma_b/\sigma < 1$, also to fulfill scale-space criteria. When $\rho = 1$, the bi-Gaussian kernel will degenerate to a Gaussian kernel. The second order derivative

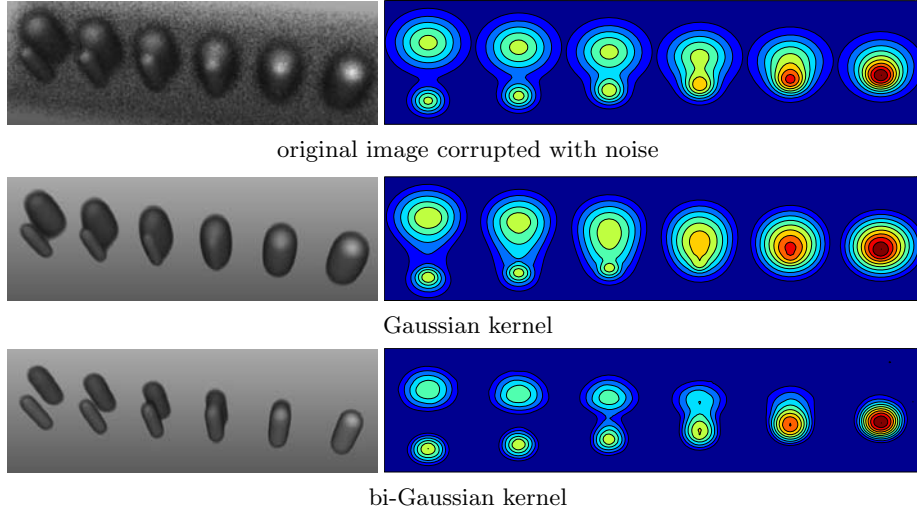


Fig. 2. 3D synthetic image filtering using the Krissian-inspired vesselness filter with different kernels, the left column is the 3D visualization and the right column corresponds to the contours of 2D cross-sections located at the axial midpoint.

of the Gaussian and bi-Gaussian kernel are depicted in Figure 1. It can be noticed that disturbances close to the vessel are not inside the kernel. More details will be published later.

We adopt the modified Krissian vesselness filter from Equation (4), but with the bi-Gaussian function as the underlying kernel to compute the Hessian and its eigenvalues, resulting in a vesselness function $V_{BG}^{med}(\sigma, x)$. To show the difference between V^{med} and V_{BG}^{med} we have plotted their vesselness responses to a synthetic object in Figure 2.

2.4 Strain energy vesselness

We have previously proposed a Strain Energy (SE) filter based on stress-strain principles from mechanics to measure vesselness [4]. The above filters assumed a simplified cylindrical vessel model with a Gaussian profile, which the SE filter tries to remedy.

The Hessian matrix is considered a stress tensor from solid mechanics, and decomposed in a mean stress component and an anisotropic component. Three orthogonal tensor invariants (measures) can be derived from this decomposition, each measuring an independent descriptor of material distortion, or in our context image structure. Translated into images they measure intensity contrast, structure strength (related to Frangi's \mathcal{S} measure), and shape. These measures are combined with a measure of intensity continuity along the vessel, and a measure to ensure the dominance of second-order over first-order derivatives to suppress undesired step edges (e.g. the lung boundary). This was finally com-

binned into a vesselness measure as follows:

$$V^{\text{SE}}(\sigma, x) = \begin{cases} 0 & \frac{1}{3}(\lambda_1 + \lambda_2 + \lambda_3) > -\alpha\lambda_m \\ \exp\left(-\beta\frac{\|\nabla I\|}{\lambda_m}\right)\rho(\mathcal{H}, \nu)V^\kappa(x) & \text{otherwise} \end{cases} \quad (6)$$

with λ_m the maximum eigenvalue, $(\lambda_1 + \lambda_2 + \lambda_3)$ the brightness contrast term, $\|\nabla I\|/\lambda_m$ the measure of relative Hessian strength to suppress step edges, $\rho(\mathcal{H}, \nu)$ the measure of structure strength, and $V^\kappa(x)$ the measure of vessel shape. More details can be found in [4]. The parameters $0 \leq \alpha < 1$, $\beta > 0$, $-1 \leq \nu \leq 0.5$, and $\kappa > 0$ are user-defined parameters.

2.5 Conversion of vesselness value to [0, 255]

The presented enhancement filters give their real-valued response each in a different range, and need to be standardized to the range $[0, 255] \subset \mathbb{N}$ as required by the organizers. All output images were first rescaled to a range $[0, 10^6]$ and rounded to the nearest integer. Subsequently, histogram equalization was employed in order to have an equal distribution of the responses at a certain threshold. Finally, the result is rescaled to the range $[0, 255]$ and stored in unsigned char format.

3 Experiments and Results

The data was made available by the VESSEL12 organizers. We did not train on any other data. Tuning of the parameters was done visually. For the multi-scale framework we selected the scales $\sigma \in \{1, 2, 3\}$ mm, used for all filters. The free parameters of V^{Frangi} were chosen as $\alpha = \beta = 0.5$ as recommended in [1] and $c = 500$ (related to the intensity range in lung CT data); V^{med} has no free parameters; $V_{\text{BG}}^{\text{med}}$: $\rho = 0.1$; and V^{SE} : $\alpha = 0.5$, $\beta = \kappa = 0.2$ and $\nu = 0.0$.

The filters V^{Frangi} , V^{med} and V^{SE} were implemented in C++ using the ITK, while the filter $V_{\text{BG}}^{\text{med}}$ was implemented in MatLab. The C++ source code is made publicly available via the toolkit ITKTools (<https://github.com/ITKTools/ITKTools>), see the tool `pxenhancement`.

3.1 Data

The data set contains both scans from asymptomatic subjects as well as scans from patients with respiratory diseases which affect the lungs in such a way that the task of identifying vessels becomes challenging.

The scans come from a variety of sources and represent a variety of clinically common scanners and protocols. The scans have been selected such that in approximately half of the scans contrast agent was used. About half of the scans contain abnormalities such as emphysema, nodules or pulmonary embolisms. The maximum slice spacing present is 1 mm and most scans are (near) isotropic. To

Table 1. Runtime in seconds. First patient, three scales, entire image.

method	time [s]
V^{Frangi}	92
V^{med}	586
$V_{\text{BG}}^{\text{med}}$	461
V^{SE}	111

ensure consistent evaluation, reference vessel segmentations for the data cannot be downloaded and will not be made available in the future.

For each scan in the VESSEL12 dataset a binary lungmask is available on the download page. Only voxels inside these lung masks will be used in the evaluation. The lung masks are provided as-is, without a claim of being perfect. We have used the lung masks to remove vesselness responses outside the mask.

3.2 Runtime

The filters V^{Frangi} and V^{SE} were run on an Intel Xeon E5620 @ 2.4 GHz, 24GB RAM, Ubuntu Linux 64 bit. The filters V^{med} and $V_{\text{BG}}^{\text{med}}$ were run on an Intel i3-2100 @ 3.1 GHz, 8GB RAM, Windows 7 64 bit. The run time for the first patient of size $512 \times 512 \times 355$ is given in Table 1. Filtering was performed on the entire image, and could be accelerated by using the lung mask to restrict computation: the lung spanned only 11% of the entire image for this patient. The Matlab implementations can obviously be sped up by moving to C++; a draft C++ implementation of the filter V^{med} decreased the runtime from 586s to 91s.

3.3 Results

Visual inspection showed that all scans were successfully enhanced. Automatic scoring was performed on the final result by the VESSEL12 organizers. The results are given in Table 2. Full results and a comparison to other participants can be found at <http://vessel12.grand-challenge.org/Results>.

Overall optimal specificity and sensitivity were (0.914, 0.960), (0.956, 0.953), (0.948, 0.953) and (0.941, 0.921), for V^{Frangi} , V^{med} , $V_{\text{BG}}^{\text{med}}$ and V^{SE} , respectively. The methods differed in their responses to sub-categories: V^{Frangi} was substantially underperforming on airways; $V_{\text{BG}}^{\text{med}}$ and V^{SE} performed best on dense abnormalities and bronchi; V^{SE} underperformed on vessels within dense abnormalities.

4 Discussion and Conclusion

The goal of our contribution was to determine what standard and generic, but fully automatic, vessel enhancement algorithms can achieve compared to the

Table 2. Results, taken from the website. A_z means area under the ROC curve. Non = non-vessels, DA = dense abnormalities, bronchi = mucus-filled bronchi, DA2 = Vessels in dense abnormality/Dense abnormalities (Contrast scans only).

Dataset	V^{Frangi}			V^{med}			$V_{\text{BG}}^{\text{med}}$			V^{SE}		
	A_z	Spec	Sens	A_z	Spec	Sens	A_z	Spec	Sens	A_z	Spec	Sens
All	0.975	0.914	0.960	0.984	0.956	0.953	0.981	0.948	0.947	0.956	0.941	0.921
01	0.990	0.901	0.985	0.995	0.931	0.985	0.986	0.882	0.963	0.976	0.918	0.963
02	0.961	0.936	0.944	0.976	0.985	0.933	0.969	0.980	0.933	0.956	0.975	0.933
03	0.980	0.950	0.967	0.989	0.977	0.967	0.988	0.968	0.945	0.977	0.963	0.934
04	0.986	0.910	0.985	0.975	0.912	0.954	0.970	0.896	0.947	0.926	0.869	0.870
05	0.976	0.912	0.963	0.984	0.967	0.963	0.987	0.960	0.953	0.969	0.960	0.953
06	0.967	0.916	0.969	0.979	0.988	0.929	0.982	0.988	0.898	0.954	0.952	0.918
07	0.987	0.789	1.000	0.993	0.886	0.990	0.985	0.862	0.990	0.914	0.841	0.867
08	0.969	0.936	0.918	0.974	0.995	0.882	0.972	0.980	0.918	0.952	0.990	0.894
09	0.975	0.918	0.949	0.983	0.973	0.929	0.987	0.984	0.929	0.952	0.978	0.908
10	0.979	0.960	0.928	0.988	0.985	0.947	0.984	0.982	0.928	0.963	0.978	0.914
11	0.987	0.965	0.950	0.990	0.984	0.944	0.988	0.988	0.931	0.961	0.996	0.931
12	0.982	0.959	0.911	0.986	0.983	0.930	0.986	0.978	0.949	0.954	0.970	0.930
13	0.985	0.967	0.930	0.990	0.991	0.912	0.994	0.991	0.921	0.983	0.986	0.956
14	0.969	0.850	1.000	0.988	0.934	0.989	0.981	0.920	0.957	0.927	0.916	0.862
15	0.973	0.966	0.933	0.986	1.000	0.944	0.993	0.993	0.944	0.970	1.000	0.867
16	0.988	0.957	0.981	0.994	0.957	0.961	0.983	0.957	0.971	0.986	0.942	0.971
17	0.979	0.909	0.966	0.972	0.960	0.914	0.970	0.949	0.931	0.942	0.939	0.897
18	0.981	0.916	0.979	0.988	0.949	0.979	0.984	0.945	0.959	0.963	0.934	0.938
19	0.970	0.934	0.972	0.995	0.979	0.972	0.995	0.983	0.966	0.976	0.983	0.945
20	0.985	0.819	0.992	0.994	0.911	0.992	0.988	0.911	0.984	0.955	0.884	0.929
Small/Non	0.952	0.893	0.947	0.979	0.935	0.956	0.978	0.931	0.953	0.964	0.934	0.953
Medium/Non	0.975	0.927	0.971	0.982	0.960	0.957	0.983	0.952	0.958	0.955	0.964	0.913
Large/Non	0.995	0.976	0.978	0.991	0.983	0.977	0.981	0.977	0.940	0.949	0.981	0.896
vs. Airways	0.738	0.615	0.691	0.940	0.855	0.908	0.941	0.856	0.912	0.953	0.950	0.930
vs. DA	0.623	0.282	0.960	0.683	0.460	0.953	0.740	0.523	0.947	0.761	0.622	0.921
vs. Bronchi	0.462	0.061	0.960	0.513	0.204	0.953	0.619	0.286	0.947	0.661	0.429	0.921
vs. DA2	0.750	0.439	0.863	0.734	0.486	0.836	0.752	0.580	0.774	0.652	0.600	0.589

competition. Overall results in terms of area under the ROC curve are good ($A_z > 0.956$) for all algorithms. The methods differed in their responses to sub-categories: V^{Frangi} was substantially underperforming on airways and bronchi; $V_{\text{BG}}^{\text{med}}$ and V^{SE} performed best on dense abnormalities and bronchi; V^{SE} was less sensitive on vessels within dense abnormalities. In general V^{SE} had a higher specificity than the other filters, at the cost of some sensitivity. It underperformed on larger vessels.

References

1. Frangi, A., Niessen, W., Vincken, K., Viergever, M.: Multiscale vessel enhancement filtering. In Wells, W., Colchester, A., Delp, S., eds.: MICCAI. Volume 1496 of

Lecture Notes in Computer Science., Springer Berlin / Heidelberg (September 1998) 130–137

2. Krissian, K., Malandain, G., Ayache, N., Vaillant, R., Troussset, Y.: Model based detection of tubular structures in 3d images. *Computer Vision and Image Understanding* **80**(2) (November 2000) 130 – 171
3. Xiao, C., Staring, M., Wang, Y., Shamonin, D., Stoel, B.: A multiscale bi-Gaussian filter for adjacent curvilinear structures detection with application to vasculature images. (2012) submitted.
4. Xiao, C., Staring, M., Shamonin, D., Reiber, J., Stolk, J., Stoel, B.: A strain energy filter for 3D vessel enhancement with application to pulmonary CT images. *Medical Image Analysis* **15**(1) (February 2011) 112 – 124